Volume 5
Number 1
January 2024
Pages 1–64

RSC Chemical Biology

rsc.li/rsc-chembio

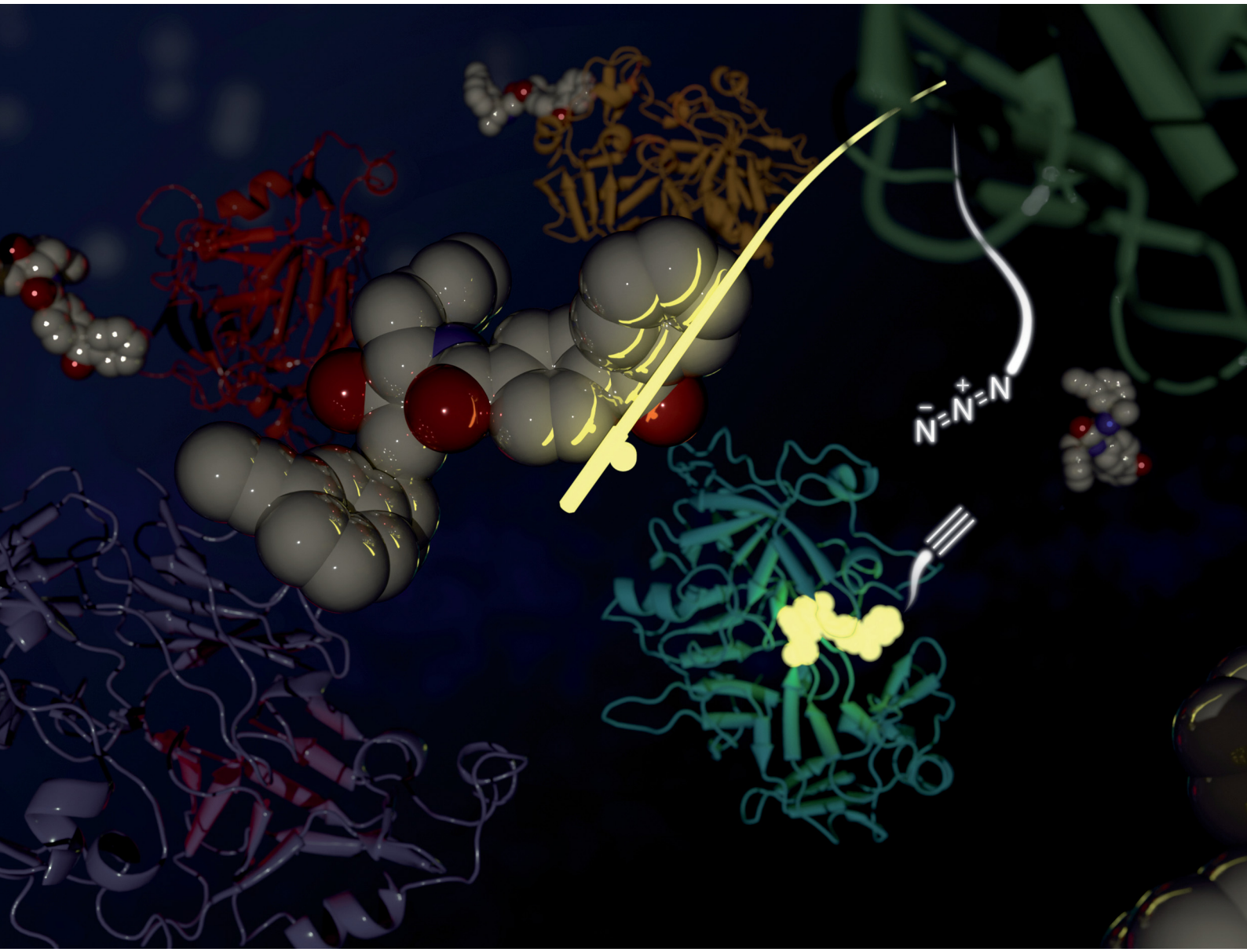

ISSN 2633-0679

ROYAL SOCIETY OF CHEMISTRY

PAPER

Paul M. O'Neill *et al.*

Design, synthesis and modelling of photoreactive chemical probes for investigating target engagement of plasmepsin IX and X in *Plasmodium falciparum*

RSC Chemical Biology

ROYAL SOCIETY OF CHEMISTRY

PAPER

View Article Online
View Journal | View Issue

Check for updates

Cite this: *RSC Chem. Biol.*, 2024, 5, 19

Design, synthesis and modelling of photoreactive chemical probes for investigating target engagement of plasmepsin IX and X in *Plasmodium falciparum*†

Monika Lisauskaitė, [a] Gemma L. Nixon, [a] Christopher M. Woodley, [a] Neil G. Berry, [a] Andy Coninckx, [a] L. Charlie Qie, [a] Suet C. Leung, [a] Donatella Taramelli, [be] Nicoletta Basilico, [ce] Silvia Parapini, [de] Stephen A. Ward, [f] Oscar Vadas, [g] Dominique Soldati-Favre, [g] W. David Hong [a] and Paul M. O'Neill *[a]

The emergence of *Plasmodium* parasite resistance to current front-line antimalarial treatments poses a serious threat to global malaria control and highlights the necessity for the development of therapeutics with novel targets and mechanisms of action. Plasmepsins IX and X (PMIX/PMX) have been recognised as highly promising targets in *Plasmodium* due to their contribution to parasite's pathogenicity. Recent research has demonstrated that dual PMIX/PMX inhibition results in the impairment of multiple parasite's life cycle stages, which is an important feature in drug resistance prevention. Herein we report novel hydroxyethylamine photoaffinity labelling (PAL) probes, designed for PMIX/PMX target engagement and proteomics experiments in *Plasmodium* parasites. The prepared probes have both a photoreactive group (diazirine or benzophenone) for covalent attachment to target proteins, and a terminal alkyne handle allowing their use in bioorthogonal ligation. One of the synthesised benzophenone probes was shown to be highly promising as demonstrated by its outstanding antimalarial potency (IC_{50} = 15 nM *versus* D10 *P. falciparum*) and its inhibitory effect against *Pf*PMX in an enzymatic assay. Molecular docking and molecular dynamics studies show that the inclusion of the benzophenone and alkyne handle does not alter the binding mode compared to the parent compound. The photoaffinity probe can be used in future chemical proteomics studies to allow hydroxyethylamine drug scaffold target identification and validation in *Plasmodium*. We expect our findings to act as a tool for future investigations on PMIX/PMX inhibition in antimalarial drug discovery.

Received 29th June 2023,
Accepted 27th October 2023

DOI: 10.1039/d3cb00109a

rsc.li/rsc-chembio

Open Access Article. Published on 13 11 2023. Downloaded on 2026-02-13 7:32:24.
This article is licensed under a Creative Commons Attribution 3.0 Unported Licence.

Introduction

Malaria is a life-threatening infectious disease caused by protozoan parasites of *Plasmodium* genus. It has been part of human history for thousands of years, yet its threat to the health and wellbeing of people worldwide remains of great concern today.[1–3] In 2021 alone, there were 247 million estimated malaria cases and 619 000 associated deaths – 76% of which occurred in children under the age of five.[4] Currently, the front-line antimalarial treatments are artemisinin combination therapies (ACTs). However, the extensive use of ACTs has resulted in *Plasmodium* resistance against artemisinin and its derivatives.[5–11] This poses a serious threat to global malaria control and aspirations of disease elimination. Due to the life-threatening nature of the disease, the resistance emergence to current treatments is extremely daunting and calls for the development of novel antimalarial drugs with unexplored mechanisms of action.

[a] *Department of Chemistry, University of Liverpool, Liverpool, L69 7ZD, UK. E-mail: pmoneill@liverpool.ac.uk*
[b] *Dipartimento di Scienze Farmacologiche e Biomolecolari (DISFEB), Università degli Studi di Milano, 20133, Milano, Italy*
[c] *Dipartimento di Scienze Biomediche, Chirurgiche e Odontoiatriche, Università degli Studi di Milano, 20133, Milano, Italy*
[d] *Dipartimento di Scienze Biomediche per la Salute, Università degli Studi di Milano, 20133, Milano, Italy*
[e] *Affiliated to Centro Interuniversitario di Ricerche sulla Malaria/Italian Malaria Network (CIRM-IMN), Università degli Studi di Camerino, Italy*
[f] *Department of Tropical Disease Biology, Liverpool School of Tropical Medicine, Liverpool, L3 5QA, UK*
[g] *Department of Microbiology and Molecular Medicine, Faculty of Medicine, CMU, 1 rue Michel-Servet, CH-1211 Genève 4, Switzerland*

† Electronic supplementary information (ESI) available. See DOI: https://doi.org/10.1039/d3cb00109a

© 2024 The Author(s). Published by the Royal Society of Chemistry

Open Access Article. Published on 13 11 2023. Downloaded on 2026-02-13 7:32:24.
This article is licensed under a Creative Commons Attribution 3.0 Unported Licence.

Since artemisinin resistance was first reported in 2008, the scientific community responded with a rise in antimalarial high-throughput screening campaigns both in academia and pharmaceutical companies.[5,12–15] This resulted in identification of thousands of starting points for hit to lead antimalarial drug optimisation. Additionally, the importance of their target identification has been recognised to allow the monitoring of potential resistance acquisition mechanisms and development. One such protein group – aspartic proteases – has been recognised as a promising target in *Plasmodium falciparum* due to its contribution to parasite's pathogenicity.[16–18] Overall, the parasite has ten aspartic proteases named plasmepsins I–X (PMI-X) that are involved in important biological processes.[16] Plasmepsins IX and X are of a particular interest due to their necessity for parasite survival and targeting of the symptomatic intraerythrocytic life cycle stage (erythrocyte invasion and egress).[19–21] PMIX is important in red blood cell (RBC) invasion and parasitophorous vacuolar membrane (PVM) set up, while PMX is required for both RBC invasion and egress.[16,19] PMX inhibition can trap the parasite within PVM and RBCs.[20] In addition to this, PMX is also expressed in the sexual stage of *P. falciparum* where its inhibition is known to affect the parasite egress from gametocytes and the invasion of vector's midgut.[20] PMX inhibition also interferes with parasite's progression from the liver to RBCs either through merosome formation blocking or effect on their function.[20]

Dual PMIX/PMX inhibition is considered a promising approach in antimalarial drug discovery due to its effect on blood stage *Plasmodium* (PMIX/PMX) as well as sexual and liver stage parasite (PMX). Such dual target inhibition can result in a lower risk of drug resistance acquisition. Therefore, development of such therapeutics is being explored and has been reported in the literature.[20,22] Hydroxyethylamine derivatives have previously been studied as potential antimalarials targeting plasmepsins due to their pharmacophore structural similarity to aspartic protease substrates.[23–26] The effect that the hydroxylamine scaffold has on plasmepsin function has been demonstrated by compound **49c** which was shown to prevent intraerythrocytic parasite's release from the PVM and host RBCs, suggesting that the drug acts as a PMX inhibitor (Fig. 1).[20,25] It was also capable of inhibiting erythrocyte invasion after 5 hours of treatment, suggesting that it might be acting as a dual PMIX/PMX inhibitor. **49c** was further tested in a mouse model infected with *P. berghei*, which showed both parasite clearance in infected mice and interreference with disease transmission – the drug caused blocking of oocyst formation in Anopheles mosquito's midgut following its blood meal. Here we report the development of novel 'clickable' photoaffinity labelling (PAL) probes based on the hydroxylamine scaffold, that will enable bioorthogonal ligation and target protein identification within living parasites. This approach will provide solid *in vitro* proof of principle for selective engagement of plasmepsin IX/X over other know plasmepsin targets.[21]

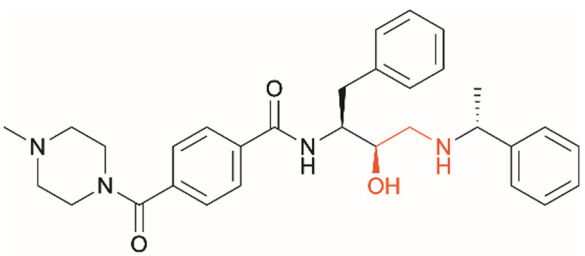

49c

$IC_{50\ (NF54)}$ = 0.6 nM (72 h)

Fig. 1 Hydroxyethylamine (red) containing PMIX/PMX inhibitor **49c** and its reported antimalarial activity against chloroquine-resistant *Plasmodium* strain NF54 after 72 hours of treatment (activity data measured in house *versus* the D10 and W2 strains of *Plasmodium falciparum* are listed in Table 1 (*vide infra*)).[20,25]

Results and discussion

Design and synthesis of diazirine photoaffinity probes

The development of 'clickable' PAL ligands for drug target identification remains challenging as two additional motifs (PAL warhead and ligation handle) have to be incorporated/merged within the ligand through an extensive knowledge of SAR. For this reason, the design of our hydroxyethylamine photoaffinity probes was focused on three key structural aspects. Firstly, in order to avoid compromising the scaffold's antimalarial activity, no chemical modifications were performed on the hydroxyethylamine moiety. The *S*,*R* chirality of this class of compounds is known to be necessary for maintaining good potency and was not altered during the probe development process.[25] Secondly, the attachment site of the photoreactive groups had to be placed either on the left-hand side or the right-hand side of the molecule based on our understanding of the structure–activity relationship (SAR). As noted, in order for the probes to be compatible with bioorthogonal ligation, incorporation of a terminal alkyne handle in the structure was also a key design element.

Photoaffinity probes **1a** and **1b** were specifically designed to incorporate diazirine moieties into their structures (Fig. 2). The photoreactive diazirine group was prioritised over other alternatives due to its small size, long excitation wavelengths, high photocrosslinking efficiency, relatively high thermal/chemical stability, and commercial availability.[27] Both aromatic (**1a**) and aliphatic (**1b**) diazirines were chosen for investigation. In probe **1a**, the alkyne handle was attached at the piperazine as structural changes on cyclic/tertiary amides appeared to be tolerated based on the inhibitor's SAR. The aromatic diazirine was incorporated into the right-hand side to mimic the benzyl substituent of **49c** that was shown to tolerate both *para* and *meta* substitution with methoxy, fluoro and nitrile functionalities.[25] Probe **1b** utilised a diazirine linker with a minimalistic design, which was anticipated to be less bulky and increase the likelihood of avoiding potency loss.

The synthesis of **1a** involved a three-part strategy encompassing the preparation of a diazirine-containing amine **5**, the synthesis of a carboxylic acid **8** incorporating a terminal alkyne, and the amide coupling between the two compounds to yield

© 2024 The Author(s). Published by the Royal Society of Chemistry

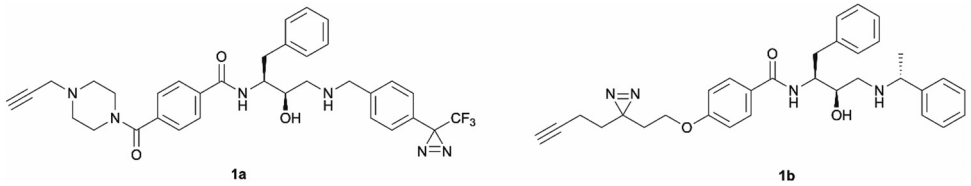

Fig. 2 Design of aromatic (**1a**) and aliphatic (**1b**) diazirine photoaffinity probes prioritised for synthesis and biological activity evaluation in *P. falciparum*.

Open Access Article. Published on 13 11 2023. Downloaded on 2026-02-13 7:32:24.
This article is licensed under a Creative Commons Attribution 3.0 Unported Licence.

the photoaffinity probe **1a** (Scheme 1). Amine preparation began with ring-opening of epoxide **2** yielding an inseparable mixture of hydroxyethylamine moiety containing intermediate **3** and cyclic byproduct **4** (structure determined following amine deprotection). The crude mixture was subjected to an overnight HCl assisted Boc deprotection in DCM. By taking advantage of the polarity difference between amine **5** and byproduct **4**, a separation method involving product precipitation was employed, which allowed successful isolation of the desired product **5** and facilitated the elucidation of the structure of the byproduct **4**. Reports of *N*-Boc-epoxide cyclisation explaining the observed byproduct formation can be found in the literature where it has been shown that the cyclic intermediate can be obtained by a 5-*exo* ring-opening reaction of the epoxide.[28] Since the purification of the Boc-protected intermediate **3** was found to be unnecessary for obtaining pure amine, the tandem approach of epoxide opening and deprotection was employed for the synthesis of all other probes that required this step (*vide infra*). It is worth noting that despite the formation of a polar byproduct being observed by TLC in other epoxide opening reactions, its isolation or further studies on conditions required to prevent this intramolecular byproduct formation were not performed as it did not show significant interference with the synthesis or purification of the HCl amine salts.

The synthesis of the carboxylic acid **8** began with an oxalyl chloride/DMF assisted amide coupling reaction between the 4-(methoxycarbonyl)benzoic acid **6** and 1-(prop-2-yn-1-yl)piperazine to allow the introduction of an alkyne handle into the probe structure. Intermediate **7** was then subjected to NaOH catalysed ester hydrolysis affording intermediate **8**. Following the synthesis of both amine **5** and carboxylic acid **8**, HATU activated amide coupling was performed to yield the desired photoaffinity probe **1a**.

For the synthesis of the aliphatic diazirine photoaffinity probe **1b**, a minimalistic diazirine substituent first had to be prepared (Scheme 2). The synthetic route commenced with an alkyne handle incorporation to ethyl acetoacetate **9** yielding intermediate **10** which then underwent ketone protection to produce **11**. Isolation of intermediates **10** and **11** was achieved in 74% and 89% yields, respectively, which was comparable to literature reports.[29,30] This was then followed by ester reduction with $LiAlH_4$ to give the hydroxy intermediate **12** which was deprotected under acidic conditions affording ketone **13**. The ketone was then converted to diazirine **14** by treating it with

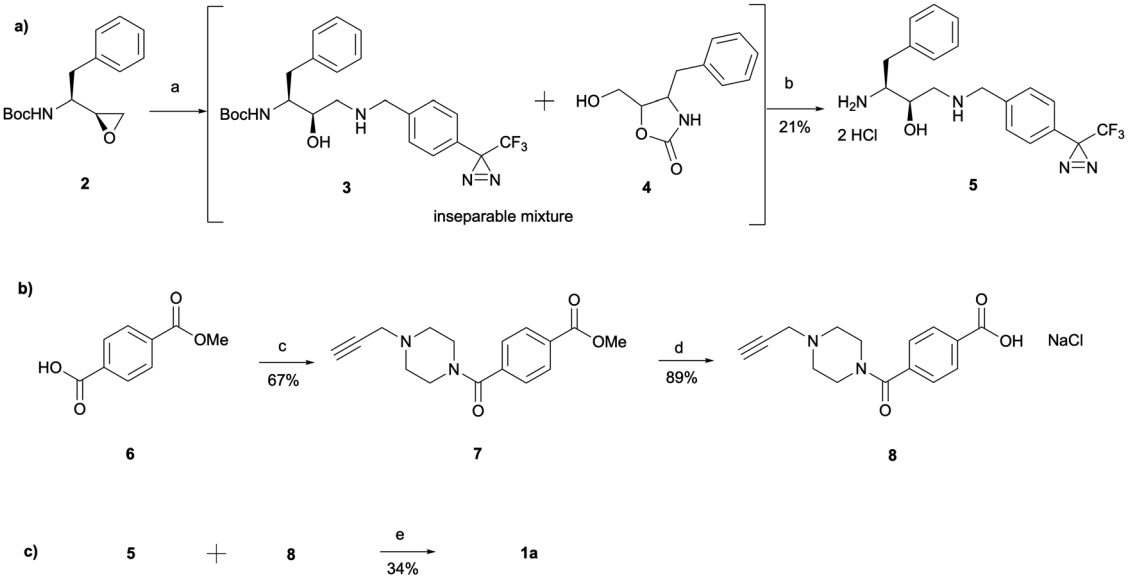

Scheme 1 Synthesis of probe **1a** consisting of three main parts: (a) amine synthesis, (b) carboxylic acid synthesis and (c) amide coupling between the two. *Reagents and conditions*: (a) (4-(3-(Trifluoromethyl)-3*H*-diazirin-3-yl)phenyl)methanamine, Et_3N, MeOH, 60 °C, 6 h; (b) HCl 4 M in dioxane, DCM, r.t., o/n; (c) oxalyl chloride, DCM, DMF, r.t., 3 h, followed by 1-(prop-2-yn-1-yl)piperazine, THF, r.t., 1.5 h; (d) NaOH, MeOH, 60 °C, 3 h, followed by HCl; (e) HATU, 4-ethylmorpholine, DMSO, r.t., o/n.

© 2024 The Author(s). Published by the Royal Society of Chemistry

Open Access Article. Published on 13 11 2023. Downloaded on 2026-02-13 7:32:24.
This article is licensed under a Creative Commons Attribution 3.0 Unported Licence.

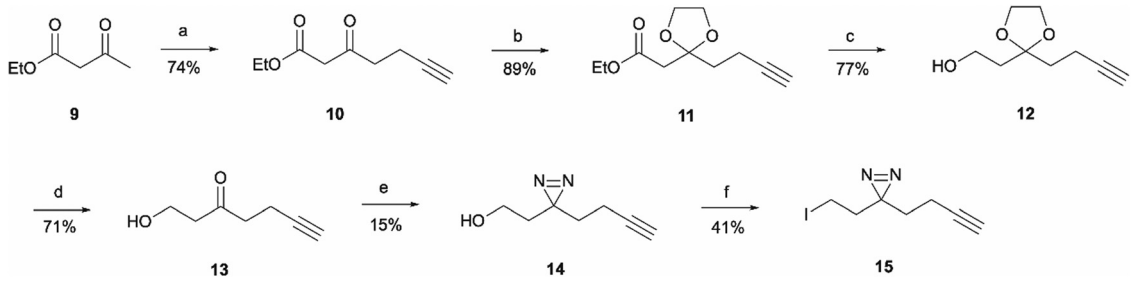

Scheme 2 Synthesis of minimalistic terminal alkyne-containing diazirine linker. *Reagents and conditions*: (a) *n*-BuLi, DIPA, THF −78 °C for 15 min before addition of **9**, then add and stir for 30 min at 0 °C; add propargyl bromide at 0 °C followed by r.t., o/n; (b) Ethylene glycol, triethyl orthoformate, TsOH·H_2O, r.t., o/n; (c) $LiAlH_4$, THF, 80 °C, 2 h; (d) TsOH·H_2O, acetone/water (5 : 1), 75 °C, 6 h; (e) 7 M NH_3 in MeOH, NH_2OSO_3, o/n followed by I_2, Et_3N, MeOH, 0 °C, 1 h; (f) I_2, PPh_3, imidazole, THF, r.t., 4 h.

7 M ammonia in methanol and hydroxylamine-*O*-sulfonic acid. This results in the formation of diaziridine that can be further oxidised with iodine in the presence of triethylamine.[31] The performed synthesis allowed diazirine **14** isolation in a 15% yield. It is worth noting that the use of 7 M ammonia in methanol solution normally results in lower yields but is more convenient and safe to handle, while higher yields of 40–80% are achievable when liquid ammonia is employed.[32–34] The formed diazirine intermediate underwent alcohol conversion to iodide **15** that could be used in S_N2 reactions as the electrophile.

15 was incorporated into the main probe pharmacophore as outlined in Scheme 3. Similarly to the synthesis of **1a**, the route for the preparation of photoaffinity probe **1b** consisted of three main parts: left-hand side carboxylic acid synthesis, right-hand side amine synthesis, and amide coupling between the two. Synthesis of the carboxylic acid **17** began with an S_N2 reaction between methyl 4-hydroxybenzoate and the prepared minimalistic linker **15**, affording intermediate **16** in a 23% yield. Unfortunately, even after heating at 60 °C for 48 hours, the formation of ether **16** was still in an undesired low yield with a significant proportion of starting material remaining. The ester intermediate **16** was then hydrolysed with NaOH affording the left-hand side building block **17** in a 20% yield. The acid **17** was precipitated using HCl and was used in the next step without further purification. Synthesis of the right-hand side amine building block followed a similar procedure as that reported for the synthesis of amine **5**. In a similar fashion to intermediate **3**, Boc-protected intermediate **18** could not be purified due to the formation of byproduct of almost identical polarity. Crude **18** was therefore used in the HCl mediated Boc deprotection to

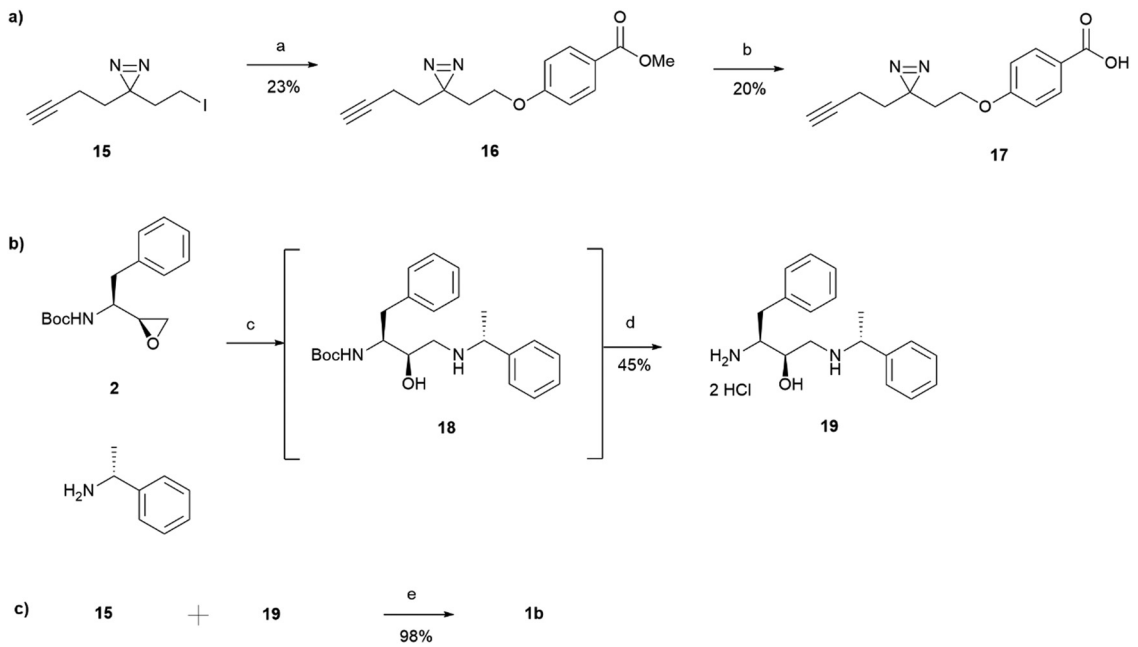

Scheme 3 Synthesis of probe **1b** consisting of three main parts: (a) carboxylic acid synthesis, (b) amine synthesis and (c) amide coupling between the two. *Reagents and conditions*: (a) Methyl 4-hydroxybenzoate, K_2CO_3, DMF, 60 °C, 48 h; (b) NaOH, MeOH, 50 °C for 3.5 h, then r.t. overnight and 50 °C for further 24 hours followed by HCl (c) (*R*)-1-phenylethan-1-amine, MeOH, 65 °C, o/n; (d) HCl 4 M in dioxane, DCM, r.t., o/n; (e) HATU, 4-ethylmorpholine, DMSO, r.t., o/n.

© 2024 The Author(s). Published by the Royal Society of Chemistry

Open Access Article. Published on 13 11 2023. Downloaded on 2026-02-13 7:32:24.
This article is licensed under a Creative Commons Attribution 3.0 Unported Licence.

afford amine **19** in a 45% yield. HATU activated amide coupling between carboxylic acid **17** and amine **19** afforded the desired photoaffinity probe **1b** in a 98% yield.

Design and synthesis of benzophenone photoaffinity probes

Benzophenone was also investigated as an alternative photoaffinity group to the diazirine to probe the effect of the different substitutions on antimalarial activity. The photoreactive group's compatibility with synthetic strategies allowing aromatic ring incorporation into the drug core structure could be exploited on our scaffold. The more desired position for benzophenone incorporation was the left-hand side of the molecule where *N*-methyl piperazinyl in **49c** was replaced by an unsubstituted phenyl group. With this in mind, probes **20a–20d** were designed (Fig. 3). Probe **20a** was expected to allow the evaluation of the effect that incorporation of benzophenone has on the scaffold's potency, while compounds **20b–20d** would explore the most suitable position for alkyne ligation handle attachment.

The synthesis of probe **20a** was a simple one step amide coupling reaction between acid **21** and the previously synthesised amine hydrochloride salt **19** (Scheme 4). The desired photoaffinity probe was isolated in a 62% yield.

Probes **20b** and **20c** were proposed as the SAR suggests that *meta* and *para* substitution at the right-hand side ring should be tolerated.[25] This was therefore identified as the most promising approach for alkyne handle attachment. In order to prepare the proposed photoaffinity probes, right-hand side amines containing an alkyne handle had to be synthesised (Scheme 5) first. The synthesis began with Boc protection of amine **22a**/**22b** to yield intermediates **23a**/**23b** in reasonably high yields of 71% and 89%, respectively. **23a**/**23b** were then subjected to Sonogashira coupling to introduce the alkyne handles. The procedure consisted of two main parts: trimethylsilylacetylene attachment to the aromatic ring through Pd/Cu catalysis, followed by trimethylsilyl group removal with base to produce the final terminal alkyne intermediates **24a**/**24b** in 73% and 82% yields. The resulting amine intermediates were then deprotected to yield their hydrochloride salts **25a**/**25b** ready for coupling to the main drug pharmacophore.

Once the right-hand side amines **25a**/**25b** were synthesised, they were used in epoxide opening reactions, which similarly to those described before, resulted in the formation of crude intermediates **26a**/**26b** (Scheme 6). They were deprotected to afford the amine building blocks **27a**/**27b** in 18% and 34% yields, respectively. The prepared amines were then coupled with 4-benzoylbenzoic acid **21** to give the photoaffinity probes **20b** and **20c** in 72% and 78% yields.

The rationale behind the design of photoaffinity probe **20d** was to examine the potential of the central benzene ring as a viable option for attaching an alkyne handle. In order to introduce the terminal alkyne into the probe's structure at the desired position, a new alkyne handle containing epoxide **34** had to be synthesised (Scheme 7). The synthetic route for the epoxide preparation began with an esterification reaction that converted the carboxylic acid starting material **28** into a methyl ester **29**. The methyl ester was chosen instead of an ethyl ester or other alternatives as the subsequent chloroketone formation step was reported to work better on methyl esters in the literature.[35] The intermediate was then used in a chloromethylation reaction to afford **30** in an 85% yield. It is worth noting that in this step, reagents sodium chloroacetate and butylmagnesium chloride are used in excess for the deprotonation of the BocNH proton, avoiding enolisation and consequent racemisation of the chiral centre.[35] According to work performed by M. J Zacuto *et al.*, it is important that in this step the reaction mixture is added to the citric acid solution and not the other way around as it prevents Mg salt precipitation which would complicate the work-up procedure.[36]

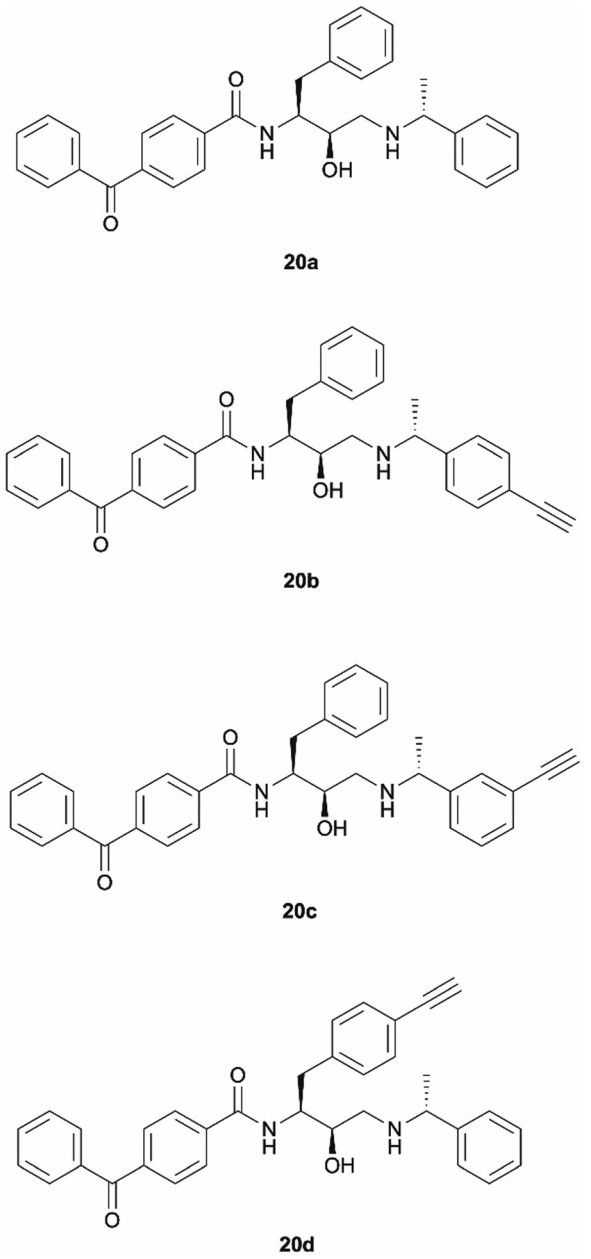

Fig. 3 Design of benzophenone probes **20a–20d** for synthesis and biological activity evaluation in *P. falciparum*.

Open Access Article. Published on 13 11 2023. Downloaded on 2026-02-13 7:32:24.
This article is licensed under a Creative Commons Attribution 3.0 Unported Licence.

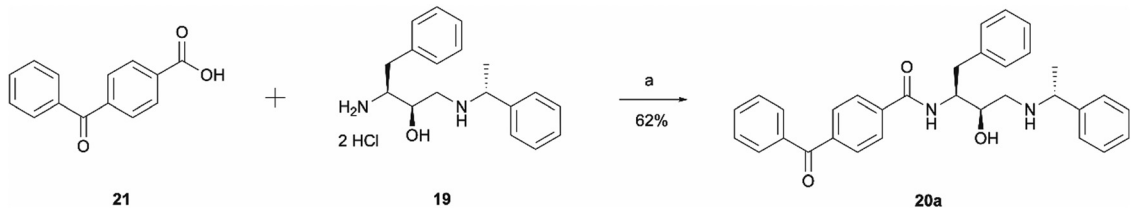

Scheme 4 Synthesis of benzophenone photoaffinity probe **20a**. *Reagents and conditions*: (a) HATU, 4-ethylmorpholine, DMSO, r.t., o/n.

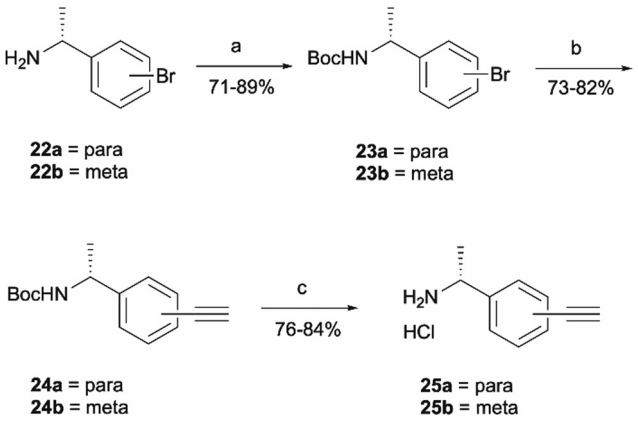

Scheme 5 Synthesis of right-hand side amines containing an alkyne handle. *Reagents and conditions*: (a) Boc_2O, Et_3N, DCM, r.t., 4 h (b) trimethylsilylacetylene, $Pd(PPh_3)_2Cl_2$, CuI, Et_3N, 70 °C, o/n, then concentrate and treat with K_2CO_3, MeOH, r.t., 3 h; (c) HCl 4 M in dioxane, MeOH, r.t., o/n.

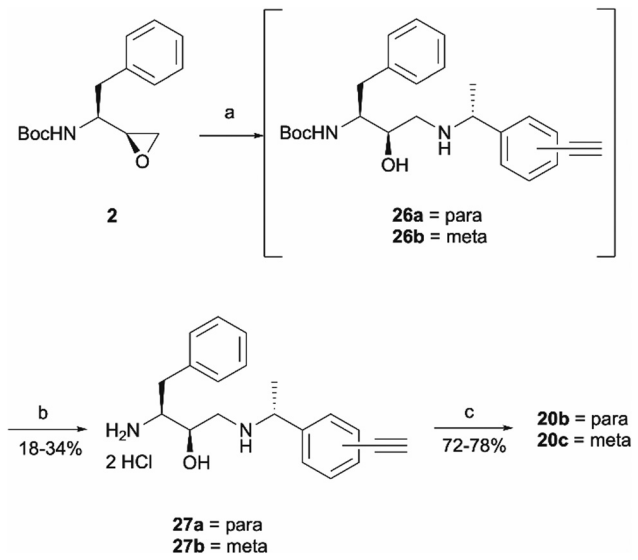

Scheme 6 Synthesis of probes **20b** and **20c**. *Reagents and conditions*: (a) Amines **25a/25b**, Et_3N, MeOH, 65 °C, o/n; (b) HCl 4 M in dioxane, DCM, r.t., o/n; (c) 4-benzoylbenzoic acid **21**, HATU, 4-ethylmorpholine, DMSO, r.t., o/n.

Once the chloromethyl functionality was introduced into the structure, the ketone in compound **30** had to be reduced to the corresponding alcohol **31** to allow the intramolecular S_N2 reaction for epoxide formation. The reduction allowed the isolation of **31** in a 31% yield and 98 : 2 d.r. The erythro (*S*,*S*) and threo (*S*,*R*) diastereomers of leucine, phenylalanine, alanine and valine derived Boc-amino epoxides can be determined through NMR analysis.[37] Ketone reduction yielding the hydroxy erythro intermediate is known to show an NH peak at 4.6 ppm in $CDCl_3$, while in the threo intermediate the same peak appears at 4.7 ppm. The diastereomeric purity of **31** was consistent in both HPLC and NMR analysis. The observed diastereoselectivity has been thoroughly discussed by O. K. Karjalainen and A. M. P. Koskinen who used a Felkin-Ahn model to propose mechanistic paths that may take place during the ketone reduction depending on the reducing agent used.[38] In our case, reasonably selective reduction was achieved using $NaBH_4$ in the formation of intermediate **31**.[38] The correct stereochemistry of the hydroxy intermediate was further confirmed by its conversion to the erythro epoxide **32** that showed the absence of any peaks at 2.99 ppm in the ^1H NMR spectra, which would correspond to the threo diastereomer methine peak. In the erythro isomer the same peak would appear at 2.84 ppm which agrees with the multiplet at 2.86–2.64 ppm.[37] Following epoxide **32** synthesis, trimethylsilylacetylene was introduced through Sonogashira coupling. The trimethylsilyl group in intermediate **33** was then removed to obtain the terminal alkyne handle which would make the probe suitable for bioorthogonal ligation. This was achieved employing a 15 min reaction with TBAF that allowed alkyne handle-containing compound **34** isolation in a 77% yield.

The prepared intermediate **34** was then used in an epoxide opening reaction, which similarly to those described in the earlier pages, resulted in a formation of crude intermediate **35** (Scheme 8). The crude Boc-protected amine was then subjected to HCl assisted deprotection affording intermediate **36** in a 44% yield. The amine salt was used in a HATU activated amide coupling reaction with the photosensitive 4-benzoylbenzoic acid **21** to afford the desired benzophenone photoaffinity probe **20d** in an 84% yield.

Antimalarial activity of photoreactive chemical probes

All the prepared photoreactive chemical probes were tested against *P. falciparum in vitro* to determine their biological activity (Table 1). Antimalarial activity was determined against chloroquine sensitive (D10) and chloroquine resistant (W2) strains by measuring parasite viability after 72 hours of incubation with the probes. The potency against D10 and W2 strains

© 2024 The Author(s). Published by the Royal Society of Chemistry

Open Access Article. Published on 13 11 2023. Downloaded on 2026-02-13 7:32:24.
This article is licensed under a Creative Commons Attribution 3.0 Unported Licence.

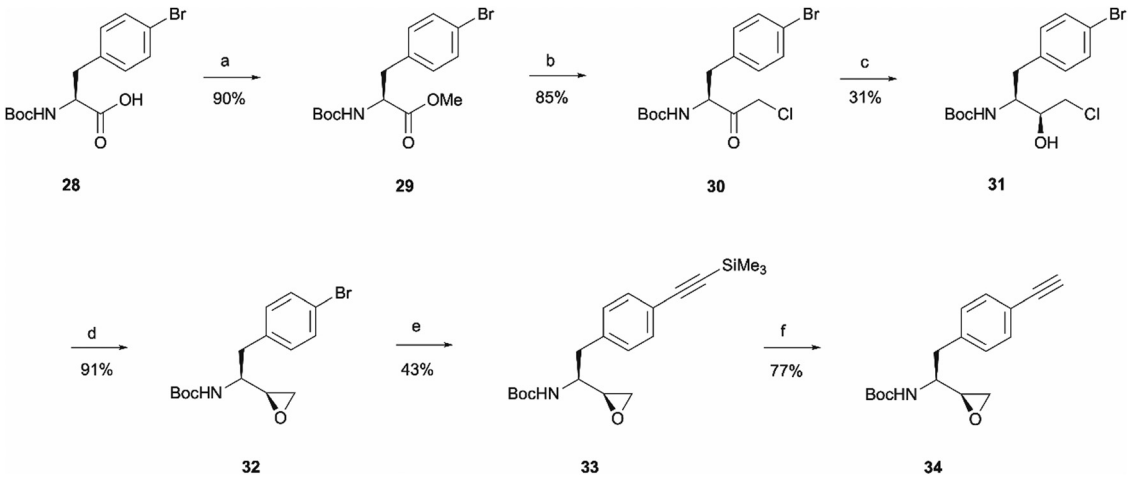

28 29 30 31 32 33 34

Scheme 7 Epoxide synthesis. *Reagents and conditions*: (a) MeI, $NaHCO_3$, DMF, r.t., o/n (b) ^{t}BuMgCl, sodium chloroacetate, Et_3N, THF, 0 °C to r.t., o/n, then aq. citric acid; (c) $NaBH_4$, EtOH, r.t., 1 h, then H^+ (d) KOH, EtOH, r.t., 1 h; (e) trimethylsilylacetylene, $Pd(PPh_3)_2Cl_2$, CuI, Et_3N, 70 °C; (f) TBAF, THF, r.t., 15 min.

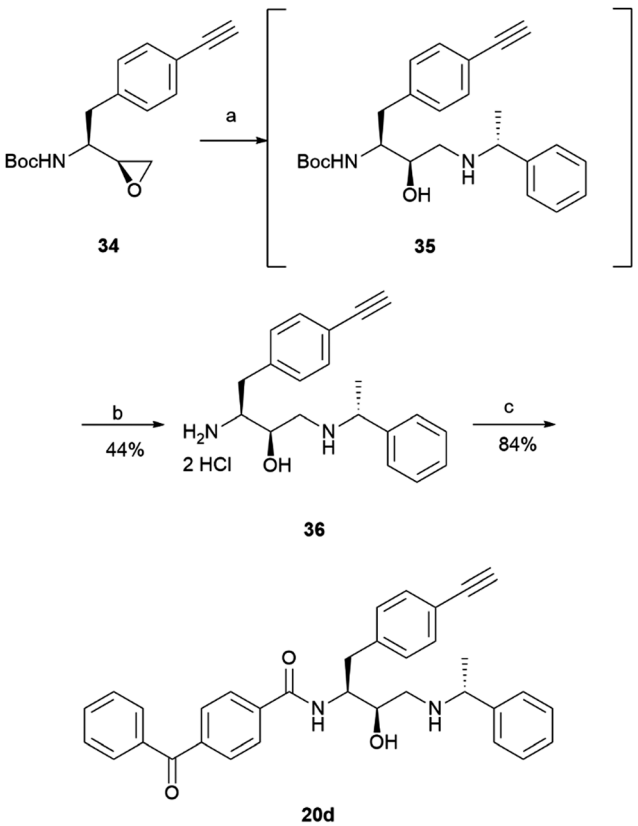

34 35 36 20d

Scheme 8 Synthesis of probe **20d**. *Reagents and conditions*: (a) 1-phenylethan-1-amine, MeOH, 65 °C, o/n; (b) HCl 4 M in dioxane, DCM, r.t., o/n; (c) 4-benzoylbenzoic acid **21**, HATU, 4-ethylmorpholine, DMSO, r.t., o/n.

was comparable for all probes. Except for the aromatic diazirine probe **1a**, all other photoaffinity probes exhibited submicromolar activity against both *P. falciparum* strains. In general, benzophenone probes were more potent than diazirine probes. Good potency of probe **20a** demonstrated that incorporation of the photoreactive benzophenone group has lower impact to the scaffold's antimalarial activity than the incorporation of diazirine group. *Meta*-substituted probe **20c** showed best activity out of all probes with an $IC_{50} < 20$ nM against both D10 and W2 strains of parasites, while the remaining benzophenone probes **20b** and **20d** exhibited 200–300 nM (IC_{50}) activity.

Table 1 Antimalarial activity of the photoreactive chemical probes measured against *P. falciparum* after 72 hours of incubation. D10 is a chloroquine sensitive parasite strain, while W2 is a chloroquine resistant strain. Chloroquine (IC_{50} = 15.53 ± 4.56 nM (D10) and 236.84 ± 81.56 (W2)) was used as a positive control in the assay (n = 3)

Probe	IC_{50} D10 (nM)	IC_{50} W2 (nM)
1a	1021.51 ± 240.04	1245.03 ± 429.57
1b	207.78 ± 86.98	195.96 ± 79.02
20a	18.29 ± 5.06	23.34 ± 3.50
20b	270.96 ± 96.61	299.58 ± 59.45
20c	15.03 ± 5.58	19.48 ± 6.54
20d	165.69 ± 45.92	204.33 ± 51.35
49c	0.77 ± 0.32	0.91 ± 0.28

Enzymatic activity of selected photoreactive chemical probes against *Pf*PMX

Three selected photoreactive chemical probes, **1b**, **20c** and **20d**, were tested in a biochemical *in vitro* assay (peptide substrate cleavage) against recombinant *Plasmodium falciparum* PMX (*Pf*PMX) with **49c** as the positive control (Fig. 4).[39] In this enzymatic assay, all three probes showed significant inhibition of *Pf*PMX activity when used at 1 μM. The two probes with the photoreactive benzophenone group, **20c** and **20d** showed similar inhibitory effect as the positive control **49c** while the diazirine incorporated probe, **1b**, showed slightly reduced inhibitory potency. These *in vitro* data show that the antimalarial activity of these probes was at least partially due to

Open Access Article. Published on 13 11 2023. Downloaded on 2026-02-13 7:32:24.
This article is licensed under a Creative Commons Attribution 3.0 Unported Licence.

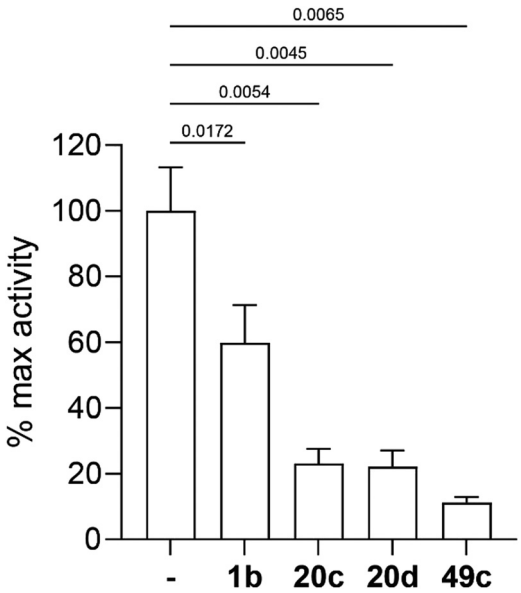

Fig. 4 Inhibition of recombinant *Pf*PMX activity by selected photoreactive chemical probes, tested on *Pf*SUB1 peptide substrate. Results shown as mean + SD (n = 3) normalised to the activity in absence of inhibitor (DMSO control). P-Values calculated by unpaired t-test.

their capability of inhibiting *Pf*PMX, one of the intended targets of **49c**.

Molecular docking and molecular dynamics studies

Having demonstrated the antimalarial activity and the enzymatic activity against *Pf*PMX of the probes, molecular docking and molecular dynamics (MD) simulations were used to determine whether the most active probe, **20c** could form sufficiently similar binding interactions to the parent compound **49c**. To generate suitable protein structures to dock the probe into, molecular dynamics studies carried out by Kesari *et al.* were replicated using **49c** docked into an experimental crystal structure of PMX co-crystallised with small molecule inhibitor WM382.[40,41] Triplicate 100 ns MD production runs were carried out and used to calculate molecular mechanics/Poisson-Boltzman surface area (MM/PBSA) binding free energy for the final 20 ns of the simulation and to determine a lowest energy binding mode.[42,43] In agreement with Kesari *et al.*, **49c** formed stable H-bonding interactions with Asp266 and Asp457 of the catalytic dyad (Fig. 5A–B), while crucially stabilising the flap region by a hydrogen bond between the central amide and Ser313 in our MD simulation.[40,44] Decomposition of these interactions' contribution to binding free energy suggests that

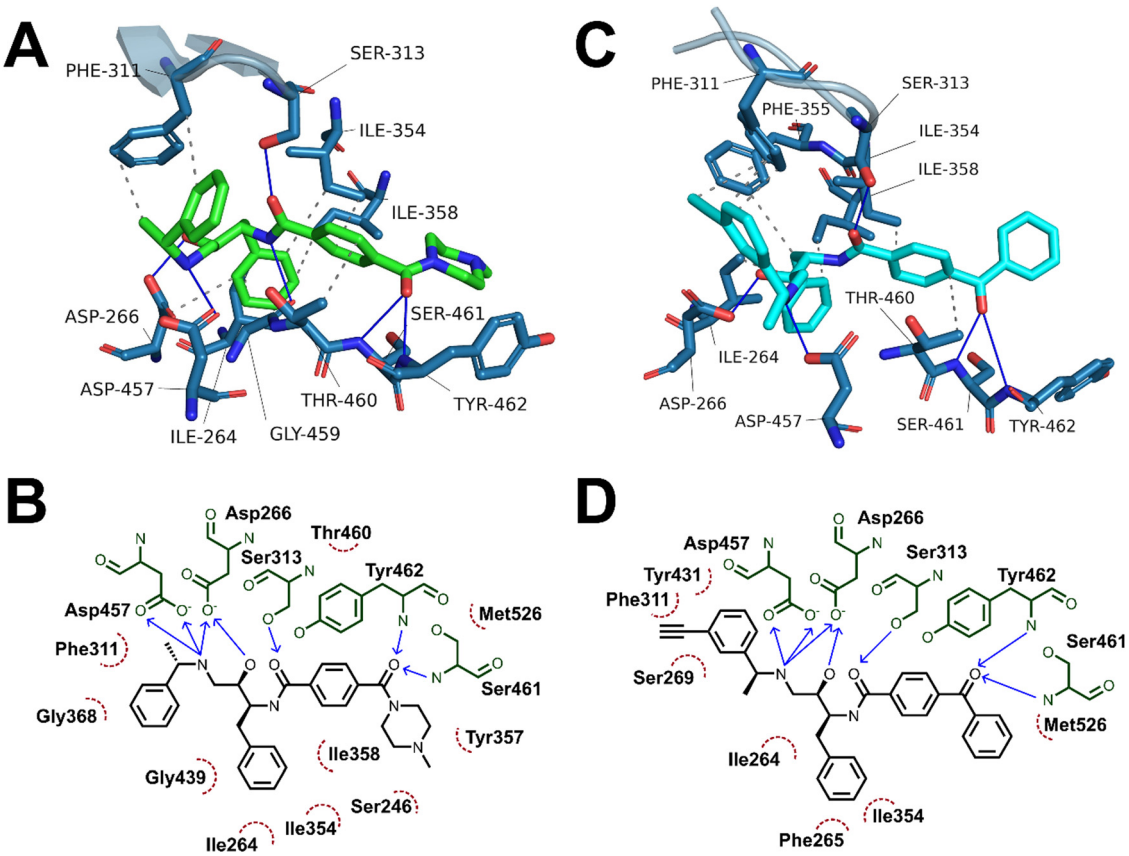

Fig. 5 (A) and (C) Interaction analyses of end-state binding modes of **49c** (A, green sticks) and **20c** (cyan sticks) in PMX. Binding site residues are shown as blue sticks, the flap region is shown as a blue cartoon representation, hydrogen bonds are shown as blue lines, hydrophobic interactions are shown as dotted grey lines. Interactions were detected using the protein ligand interaction profiler tool. (B) and (D) 2D representations of non-covalent interactions between **49c** (A) and **20c** (B) with binding site residues. Binding site residues are shown in green, hydrophobic interacting residues are depicted by red, dotted arcs, hydrogen bond donors are depicted as blue arrows point from donor to acceptor.

© 2024 The Author(s). Published by the Royal Society of Chemistry

Open Access Article. Published on 13 11 2023. Downloaded on 2026-02-13 7:32:24.
This article is licensed under a Creative Commons Attribution 3.0 Unported Licence.

the interaction between the charged amine and the deprotonated aspartate residues are the greatest contributing interaction to binding energy (Fig. S1, ESI†). Additional interactions detected over the course of the simulation included hydrogen bonds to Ser461 and Tyr462 and detected hydrophobic interactions with Ile354, Phe311, Thr460 and Tyr462.

The probes synthesised in this work were initially docked into a representative structure from the lowest energy MD run of **49c** (interaction analyses of all docked probes is provided in the ESI†). The highest ranking pose of **20c** was prepared for MD simulation using the same method and settings as **49c**. Production MD runs of 100 ns were ran in triplicate and analysed by MM/PBSA and clustering methods. Two of the three MD simulations of **20c**, runs 1 and 3, converged to similar MM/PBSA predicted binding energies, while the binding mode generated in run 2 had weaker binding energy.

The average MM/PBSA binding energy for **20c** run 1 was similar to the value obtained for **49c** (-426.2 ± 26.2 *versus* -442.727 ± 16.8 kJ mol^{-1}) with greatest contribution through the catalytic dyad, consistent with the comparable *in vitro* antimalarial activity. Similar to **49c**, **20c** likely forms stable hydrogen bonding interactions between ligand and the catalytic aspartate residues as well as the key flap-stabilising interaction between Ser313 and the central amide carbonyl (Fig. 5C–D). Additional stable hydrogen bonding interactions with Ser461 and Tyr462, as well as a network of hydrophobic interactions were also detected in the same MD run using **20c**. The predicted binding energy of **20c** run 3 was also similar to **49c** (-429.4 ± 19.3 kJ mol^{-1}) and maintained stable interactions with both aspartate residues and Ser313, however the terminal ring of the benzophenone bound further into the hydrophobic pocket defined by Tyr462. This resulted in hydrogen bonds between Ser461 and Tyr462 and the benzophenone carbonyl being lost in lieu of greater hydrophobic interactions, as evidenced by greater van der Waals contribution to binding free energy (Fig. S2 and Table S1, ESI†). The left-hand-side benzylamine group in **20c** was observed to adopt an altered conformation compared to **49c** – where in the predicted binding mode of **49c** the methyl group points towards Phe311, in **20c** the alkyne handle points towards Phe311 and the methyl group points towards the protein surface. This can be rationalised by the formation of stabilising hydrophobic interactions between the alkyne and the phenyl ring of Phe311 (Fig. 5C–D) – this is supported by the greater contribution of Phe311 to the calculated binding free energy of **20c** *versus* **49c**.

A detailed summary of detected interactions and details of MM/PBSA analysis are provided in the ESI† (Tables S1 and S2). These molecular docking and molecular dynamics studies support that the *in vitro* activity of **20c** likely occurs by a similar mechanism of action to **49c** and suggest that **20c** may be used as a chemical probe in target engagement and elucidation studies for antimalarial compounds related to **49c**.

Conclusions

In this study, we present the development of novel aspartic acid protease photoaffinity chemical probes containing photoreactive groups and a terminal alkyne moiety for bioorthogonal ligation in biological systems. By drawing on our understanding of the antimalarial SAR, we have managed to achieve the incorporation of photoreactive label and ligation handle within the parent scaffold whilst maintaining nanomolar drug potency. The incorporation of photoreactive groups is expected to allow covalent probe attachment to near proximity amino acid residues in the targeted proteins, while the inclusion of the terminal alkyne group will enable efficient and selective isolation of proteins under investigation through 'click' chemistry. Through this PAL based chemical proteomics approach, we will be able to provide a quantitative assessment of the degree of in-parasite plasmepsin labelling and determination of drug selectivity against plasmepsins IX and X over the other variants.[21] Among the synthesised probes, **20c** showed the most promising results in terms of antimalarial activity ($IC_{50} < 20$ nM) and proof-of-concept enzymatic inhibitory activity against one of the intended targets, *Pf*PMX. Subsequently, molecular docking and molecular dynamics studies in PMX demonstrated that the inclusion of the photoreactive group and terminal alkyne handle did not significantly alter the binding mode of the probe's scaffold in comparison to the parent **49c**, further validating its potential.

Author contributions

The project was conceptualised by ML, GN, SAW, WDH, CW, NBe, AC, LCQ, DT, SP and PMO'N. It was supervised by PMO'N, GN, WDH and NBe. The manuscript was written by ML and CW, with input from PMO'N, GN, SCL, WDH and NB. ML performed photoaffinity probe design, their synthesis and associated data analysis. CW performed molecular docking and molecular dynamic studies. DT, NBa and SP performed the biological studies. OV and DSF optimised and performed the *in vitro* plasmepsin X inhibition assays. All authors have read and approved the manuscript.

Conflicts of interest

There are no conflicts to declare.

Acknowledgements

ML would like to acknowledge the EPSRC for a DTA award (EP/R513271/1), AC for a UOL GTA Award, LCQ would like to thank the University of Liverpool (UOL) for the award of an International Postgraduate Research Studentship and CW for a UOL Fellowship Award. We thank Teresa De Haro Garcia and her team from UCB UK for providing recombinant *Pf*PMX. We are also grateful to the Immunohematology and Transfusion Medicine Service, Department of Laboratory Medicine, and ASST Grande Ospedale Metropolitano Niguarda (Milan) for providing the erythrocytes for parasite cultures. This work was also supported by an MRC CiC grant (MC_PC_19045) awarded to SAW, WDH and PMO'N.

Open Access Article. Published on 13 11 2023. Downloaded on 2026-02-13 7:32:24.
This article is licensed under a Creative Commons Attribution 3.0 Unported Licence.

References

1 M. A. Phillips, J. N. Burrows, C. Manyando, R. H. van Huijsduijnen, W. C. Van Voorhis and T. N. C. Wells, *Nat. Rev. Dis. Primers*, 2017, **3**, 17050.
2 P. Jagannathan and A. Kakuru, *Nat. Commun.*, 2022, **13**, 2678.
3 J. M. Cohen, F. Okumu and B. Moonen, *Sci. Transl. Med.*, 2022, **14**, eabn3256.
4 World Health Organization, World malaria report 2022, Geneva, 2022.
5 H. Noedl, Y. Se, K. Schaecher, B. L. Smith, D. Socheat and M. M. Fukuda, *N. Engl. J. Med.*, 2008, **359**, 2619–2620.
6 E. A. Ashley, M. Dhorda, R. M. Fairhurst, C. Amaratunga, P. Lim, S. Suon, S. Sreng, J. M. Anderson, S. Mao, B. Sam, C. Sopha, C. M. Chuor, C. Nguon, S. Sovannaroth, S. Pukrittayakamee, P. Jittamala, K. Chotivanich, K. Chutasmit, C. Suchatsoonthorn, R. Runcharoen, T. T. Hien, N. T. Thuy-Nhien, N. V. Thanh, N. H. Phu, Y. Htut, K.-T. Han, K. H. Aye, O. A. Mokuolu, R. R. Olaosebikan, O. O. Folaranmi, M. Mayxay, M. Khanthavong, B. Hongvanthong, P. N. Newton, M. A. Onyamboko, C. I. Fanello, A. K. Tshefu, N. Mishra, N. Valecha, A. P. Phyo, F. Nosten, P. Yi, R. Tripura, S. Borrmann, M. Bashraheil, J. Peshu, M. A. Faiz, A. Ghose, M. A. Hossain, R. Samad, M. R. Rahman, M. M. Hasan, A. Islam, O. Miotto, R. Amato, B. MacInnis, J. Stalker, D. P. Kwiatkowski, Z. Bozdech, A. Jeeyapant, P. Y. Cheah, T. Sakulthaew, J. Chalk, B. Intharabut, K. Silamut, S. J. Lee, B. Vihokhern, C. Kunasol, M. Imwong, J. Tarning, W. J. Taylor, S. Yeung, C. J. Woodrow, J. A. Flegg, D. Das, J. Smith, M. Venkatesan, C. V. Plowe, K. Stepniewska, P. J. Guerin, A. M. Dondorp, N. P. Day and N. J. White, *N. Engl. J. Med.*, 2014, **371**, 411–423.
7 M. Imwong, K. Suwannasin, C. Kunasol, K. Sutawong, M. Mayxay, H. Rekol, F. M. Smithuis, T. M. Hlaing, K. M. Tun, R. W. van der Pluijm, R. Tripura, O. Miotto, D. Menard, M. Dhorda, N. P. J. Day, N. J. White and A. M. Dondorp, *Lancet Infect. Dis.*, 2017, **17**(5), 491–497.
8 L. Roberts, *Science*, 2016, **352**, 398–405.
9 World Health Organization, Artemisinin resistance and artemisinin-based combination therapy efficacy: status report, 2018.
10 M. Imwong, M. Dhorda, K. Myo Tun, A. M. Thu, A. P. Phyo, S. Proux, K. Suwannasin, C. Kunasol, S. Srisutham, J. Duanguppama, R. Vongpromek, C. Promnarate, A. Saejeng, N. Khantikul, R. Sugaram, S. Thanapongpichat, N. Sawangjaroen, K. Sutawong, K. T. Han, Y. Htut, K. Linn, A. A. Win, T. M. Hlaing, R. W. van der Pluijm, M. Mayxay, T. Pongvongsa, K. Phommasone, R. Tripura, T. J. Peto, L. von Seidlein, C. Nguon, D. Lek, X. H. S. Chan, H. Rekol, R. Leang, C. Huch, D. P. Kwiatkowski, O. Miotto, E. A. Ashley, M. P. Kyaw, S. Pukrittayakamee, N. P. J. Day, A. M. Dondorp, F. M. Smithuis, F. H. Nosten and N. J. White, *Lancet Infect. Dis.*, 2020, **20**, 1470–1480.
11 A. Uwimana, N. Umulisa, M. Venkatesan, S. S. Svigel, Z. Zhou, T. Munyaneza, R. M. Habimana, A. Rucogoza, L. F. Moriarty, R. Sandford, E. Piercefield, I. Goldman, B. Ezema, E. Talundzic, M. A. Pacheco, A. A. Escalante, D. Ngamije, J.-L. N. Mangala, M. Kabera, K. Munguti, M. Murindahabi, W. Brieger, C. Musanabaganwa, L. Mutesa, V. Udhayakumar, A. Mbituyumuremyi, E. S. Halsey and N. W. Lucchi, *Lancet Infect. Dis.*, 2021, **21**, 1120–1128.
12 D. Plouffe, A. Brinker, C. McNamara, K. Henson, N. Kato, K. Kuhen, A. Nagle, F. Adrián, J. T. Matzen, P. Anderson, T. Nam, N. S. Gray, A. Chatterjee, J. Janes, S. F. Yan, R. Trager, J. S. Caldwell, P. G. Schultz, Y. Zhou and E. A. Winzeler, *Proc. Natl. Acad. Sci. U. S. A.*, 2008, **105**, 9059–9064.
13 F.-J. Gamo, L. M. Sanz, J. Vidal, C. de Cozar, E. Alvarez, J.-L. Lavandera, D. E. Vanderwall, D. V. S. Green, V. Kumar, S. Hasan, J. R. Brown, C. E. Peishoff, L. R. Cardon and J. F. Garcia-Bustos, *Nature*, 2010, **465**, 305–310.
14 W. A. Guiguemde, A. A. Shelat, D. Bouck, S. Duffy, G. J. Crowther, P. H. Davis, D. C. Smithson, M. Connelly, J. Clark, F. Zhu, M. B. Jiménez-Díaz, M. S. Martinez, E. B. Wilson, A. K. Tripathi, J. Gut, E. R. Sharlow, I. Bathurst, F. El Mazouni, J. W. Fowble, I. Forquer, P. L. McGinley, S. Castro, I. Angulo-Barturen, S. Ferrer, P. J. Rosenthal, J. L. Derisi, D. J. Sullivan, J. S. Lazo, D. S. Roos, M. K. Riscoe, M. A. Phillips, P. K. Rathod, W. C. Van Voorhis, V. M. Avery and R. K. Guy, *Nature*, 2010, **465**, 311–315.
15 W. A. Guiguemde, A. A. Shelat, J. F. Garcia-Bustos, T. T. Diagana, F.-J. Gamo and R. K. Guy, *Chem. Biol.*, 2012, **19**, 116–129.
16 A. S. Nasamu, A. J. Polino, E. S. Istvan and D. E. Goldberg, *J. Biol. Chem.*, 2020, **295**, 8425–8441.
17 B. E. Sleebs, M. Gazdik, M. T. O'Neill, P. Rajasekaran, S. Lopaticki, K. Lackovic, K. Lowes, B. J. Smith, A. F. Cowman and J. A. Boddey, *J. Med. Chem.*, 2014, **57**, 7644–7662.
18 I. Russo, S. Babbitt, V. Muralidharan, T. Butler, A. Oksman and D. E. Goldberg, *Nature*, 2010, **463**, 632–636.
19 A. S. Nasamu, S. Glushakova, I. Russo, B. Vaupel, A. Oksman, A. S. Kim, D. H. Fremont, N. Tolia, J. R. Beck, M. J. Meyers, J. C. Niles, J. Zimmerberg and D. E. Goldberg, *Science*, 2017, **358**, 518–522.
20 P. Pino, R. Caldelari, B. Mukherjee, J. Vahokoski, N. Klages, B. Maco, C. R. Collins, M. J. Blackman, I. Kursula, V. Heussler, M. Brochet and D. Soldati-Favre, *Science*, 2017, **358**, 522–528.
21 P. M. Cheuka, G. Dziwornu, J. Okombo and K. Chibale, *J. Med. Chem.*, 2020, **63**, 4445–4467.
22 P. Favuzza, M. de Lera Ruiz, J. K. Thompson, T. Triglia, A. Ngo, R. W. J. Steel, M. Vavrek, J. Christensen, J. Healer, C. Boyce, Z. Guo, M. Hu, T. Khan, N. Murgolo, L. Zhao, J. S. Penington, K. Reaksudsan, K. Jarman, M. H. Dietrich, L. Richardson, K.-Y. Guo, S. Lopaticki, W.-H. Tham, M. Rottmann, T. Papenfuss, J. A. Robbins, J. A. Boddey, B. E. Sleebs, H. J. Sabroux, J. A. McCauley, D. B. Olsen and A. F. Cowman, *Cell Host Microbe*, 2020, **27**, 642–658.
23 R. Zogota, L. Kinena, C. Withers-Martinez, M. J. Blackman, R. Bobrovs, T. Pantelejevs, I. Kanepe-Lapsa, V. Ozola, K. Jaudzems, E. Suna and A. Jirgensons, *Eur. J. Med. Chem.*, 2019, **163**, 344–352.

© 2024 The Author(s). Published by the Royal Society of Chemistry

Open Access Article. Published on 13 11 2023. Downloaded on 2026-02-13 7:32:24.
This article is licensed under a Creative Commons Attribution 3.0 Unported Licence.

24 D. Nöteberg, E. Hamelink, J. Hultén, M. Wahlgren, L. Vrang, B. Samuelsson and A. Hallberg, *J. Med. Chem.*, 2003, **46**, 734–746.
25 C.-L. Ciana, R. Siegrist, H. Aissaoui, L. Marx, S. Racine, S. Meyer, C. Binkert, R. de Kanter, C. Fischli, S. Wittlin and C. Boss, *Bioorg. Med. Chem. Lett.*, 2013, **23**, 658–662.
26 K. Liu, H. Shi, H. Xiao, A. G. L. Chong, X. Bi, Y.-T. Chang, K. S. W. Tan, R. Y. Yada and S. Q. Yao, *Angew. Chem., Int. Ed.*, 2009, **48**, 8293–8297.
27 S.-S. Ge, B. Chen, Y.-Y. Wu, Q.-S. Long, Y.-L. Zhao, P.-Y. Wang and S. Yang, *RSC Adv.*, 2018, **8**, 29428–29454.
28 H. Borgohain, K. Talukdar, B. Sarma and S. K. Das, *Org. Biomol. Chem.*, 2020, **18**, 7401–7413.
29 K. Hayakawa, M. Yodo, S. Ohsuki and K. Kanematsu, *J. Am. Chem. Soc.*, 1984, **106**, 6735–6740.
30 M. Walko, E. Hewitt, S. E. Radford and A. J. Wilson, *RSC Adv.*, 2019, **9**, 7610–7614.
31 R. F. R. Church and M. J. Weiss, *J. Org. Chem.*, 1970, **35**, 2465–2471.
32 L. Wang, Z. P. Tachrim, N. Kurokawa, F. Ohashi, Y. Sakihama, Y. Hashidoko and M. Hashimoto, *Molecules*, 2017, **22**, 1389.
33 Z. Li, P. Hao, L. Li, C. Y. J. Tan, X. Cheng, G. Y. J. Chen, S. K. Sze, H.-M. Shen and S. Q. Yao, *Angew. Chem., Int. Ed.*, 2013, **52**, 8551–8556.
34 L. Wang, A. Ishida, Y. Hashidoko and M. Hashimoto, *Angew. Chem., Int. Ed.*, 2017, **56**, 870–873.
35 X. Wang, J. K. Thottathil and R. P. Polniaszek, *Synlett*, 2000, 902–904.
36 M. J. Zacuto, R. F. Dunn and M. Figus, *J. Org. Chem.*, 2014, **79**, 8917–8925.
37 D. P. Rotella, *Tetrahedron Lett.*, 1995, **36**, 5453–5456.
38 O. K. Karjalainen and A. M. P. Koskinen, *Org. Biomol. Chem.*, 2012, **10**, 4311.
39 M. A. Lowe, A. Cardenas, J.-P. Valentin, Z. Zhu, J. Abendroth, J. L. Castro, R. Class, A. Delaunois, R. Fleurance, H. Gerets, V. Gryshkova, L. King, D. D. Lorimer, M. MacCoss, J. H. Rowley, M.-L. Rosseels, L. Royer, R. D. Taylor, M. Wong, O. Zaccheo, V. P. Chavan, G. A. Ghule, B. K. Tapkir, J. N. Burrows, M. Duffey, M. Rottmann, S. Wittlin, I. Angulo-Barturen, M. B. Jiménez-Díaz, J. Striepen, K. J. Fairhurst, T. Yeo, D. A. Fidock, A. F. Cowman, P. Favuzza, B. Crespo-Fernandez, F. J. Gamo, D. E. Goldberg, D. Soldati-Favre, B. Laleu and T. de Haro, *J. Med. Chem.*, 2022, **65**, 14121–14143.
40 P. Kesari, A. Deshmukh, N. Pahelkar, A. B. Suryawanshi, I. Rathore, V. Mishra, J. H. Dupuis, H. Xiao, A. Gustchina, J. Abendroth, M. Labaied, R. Y. Yada, A. Wlodawer, T. E. Edwards, D. D. Lorimer and P. Bhaumik, *Protein Sci.*, 2022, **31**, 882–899.
41 A. N. Hodder, J. Christensen, S. Scally, T. Triglia, A. Ngo, R. W. Birkinshaw, B. Bailey, P. Favuzza, M. H. Dietrich, W.-H. Tham, P. E. Czabotar, K. Lowes, Z. Guo, N. Murgolo, M. de Lera Ruiz, J. A. McCauley, B. E. Sleebs, D. Olsen and A. F. Cowman, *Structure*, 2022, **30**, 947–961.
42 N. Homeyer and H. Gohlke, *Mol. Inf.*, 2012, **31**, 114–122.
43 R. Kumari, R. Kumar and A. Lynn, *J. Chem. Inf. Model.*, 2014, **54**, 1951–1962.
44 J. A. Henderson and J. Shen, *J. Chem. Inf. Model.*, 2022, **62**, 150–158.

© 2024 The Author(s). Published by the Royal Society of Chemistry